Mineralogy, Radioactivity and Geochemistry of the altered granite of Gabal Nikeiba area, South Eastern Desert, Egypt

Wafaa. H. Saleh

Nuclear Materials Authority, Cairo, Egypt. 530.P.O. El Maadi, Cairo, Egypt.
drwafaahosny@live.com

Abstract: The rock types in Gabal Nikeiba area are dominantly metavolcanics (lithic tuffs and crystal tuffs), tonalite, post orgonic (younger) granitic rocks, post granite dykes, veins and tertiary sediments. The young granites range in composition from monzogranite, syenogranite to alkali feldspar granite. They are the most favorable host rocks for uranium and thorium mineralization, especially in altered facies. Uranium and thorium concentrations of the studied altered granites range between 1031 and 2944, 4028 and 4030 ppm, respectively suggesting that the altered granites belong to high thorium, high uranium granites. Th/U and $^{234}U/^{238}U$ ratio indicate that the presence of more than one stage of uranium mineralization. Radioactive mineralized zone show average activity concentration of the ^{238}U (24516 $BqKg^{-1}$), ^{234}U (11937 $BqKg^{-1}$), ^{232}Th (15153.67 $BqKg^{-1}$), ^{40}K (1558.5 $BqKg^{-1}$) and ^{235}U (1101.83 $BqKg^{-1}$). The first is uranium accumulation in the studied altered granites clarified from Th/U ratio, followed by later uranium leaching from altered granites to the surrounding rocks as indicated by $^{234}U/^{238}U$ ratio. High uranium and thorium contents are mainly attributed to the presence of uranothorite, thorite, kasolite, fergusonite, ferrocolumbite and zircon in the studied altered granites. Other mineralization are also recorded such as gold, galena and fluorite. Geochemical investigations show that the studied altered granites are subjected to desilicification, albitization and silicification, several processes of alterations in the uraniferous granites, sodic or potassic metasomatism, serictization is the most common process associating with other processes of alteration. Chemical compositional variation in minerals is referred to two solid solution types, the first type when ion of higher charge substitutes for two lower charged ions to maintain charge balance. In this study, the EDX analysis indicate enrichment of Ca^{2+} (14.14%) on the account of Na^{+1} and K^{+1}. The second type is the interstitial solid solution, where some sites in the crystal structure are vacant (M- site) occupied by the other ions especially the trace elements such as Nb, Zr, Hf, REE and uranium, while the temperature range increase from 750^0C to 1000^0C. The studied highly radioactive granite zone revealed that the chondrite normalized REE patterns are different from the normal M- and W-type of tetrad effects and has complex characteristics of the two types. The first four elements (La, Ce, Pr, Nd) and the third set (Gd, Tb, Dy, Ho) exhibit a clear convex curve (M-type) while the fourth (Er, Tm, Yb, Lu) define distinct concave curves (W-type), on chondrite-normalized plots. The convex (M-type) T_1 and T_3 accompanying with concave (W-type) T_4 may be related to the physico-chemical conditions that prevailed during the alteration processes. The unusual MW-type tetrad effect could be considered as geochemical exploration method for Au mineralization of reworked plutons.

[Wafaa. H. Saleh. **Mineralogy, Radioactivity and Geochemistry of the altered granite of Gabal Nikeiba area, South Eastern Desert, Egypt.** *Nat Sci* 2019;17(5):54-67]. ISSN 1545-0740 (print); ISSN 2375-7167 (online). http://www.sciencepub.net/nature. 7. doi:10.7537/marsnsj170519.07.

Key words: Mineralogy, Radioactivity, Geochemistry, Gabal Nikeiba area, South Eastern Desert**.**

Introduction:

Uranium exploration in G. Nikeiba area is considered an important target, during the last years where the fertility criteria were planned to be applied for studying granitic rocks in the Eastern Desert. G. Nikeiba is bounded by latitude (23^0 52` 35" - $23^0$ 53` 27") N and longitude (34^0 20` 59" - $34^0$ 21` 54") E covering about 400 Km^2 Fig. (1,b). The rock types in Gabal Nikeiba area are dominantly metavolcanics (lithic tuffs and crystal tuffs), tonalite, granitic rocks (old granite and young granite), post granite dykes, veins and tertiary sediments. The young granites range in composition from monzogranite, syenogranite to alkali feldspar granite Fig. (1,c).

Abdel Gawad (2011) described the central part of the mountain as syenogranite that surrounded by qz-syenite covering the eastern, northern and western parts of G. El Nekeiba. It is dissected by many fault sets and bounded by W. Road El Sayalla that extends from the western side, passing south the mountain to the eastern side. They attributed radioactivity of the area mainly to quartz-syenite and consequently to the felsic dykes. Mainly, the hydrothermal processes control the distribution of uranium within the rocks during the final stages of crystallization of granitic magma (O'Connor et al., 1982). The origin of high U-contents in the studied rocks is mainly related to alteration of primary minerals by the action of oxidizing fluids, mobilization and redistribution by

circulating of meteoric waters in other forms (Khaleal et al., 2007). The aim of the presenter search work is to throw light on the radioactivity, mineralogy and REEs geochemistry of the altered granites in the G. El Nekeiba area.

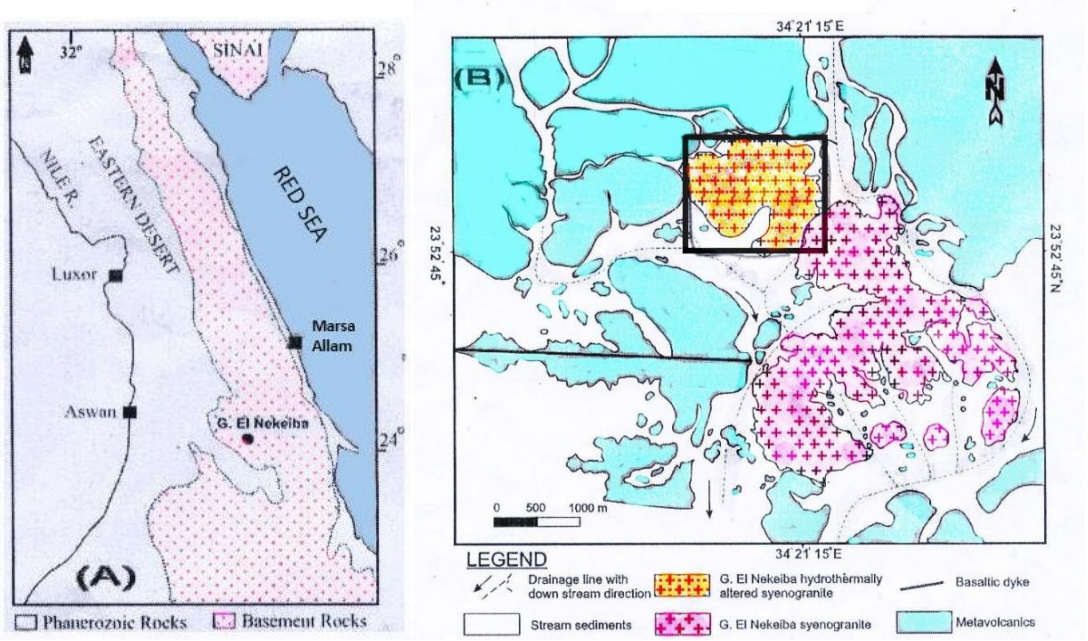

Fig. (1): A-Location map of G. El Nekieba area, B-Geological map of G Nekieba area, the in set rectangle shows the detailed area of Fig. (B)

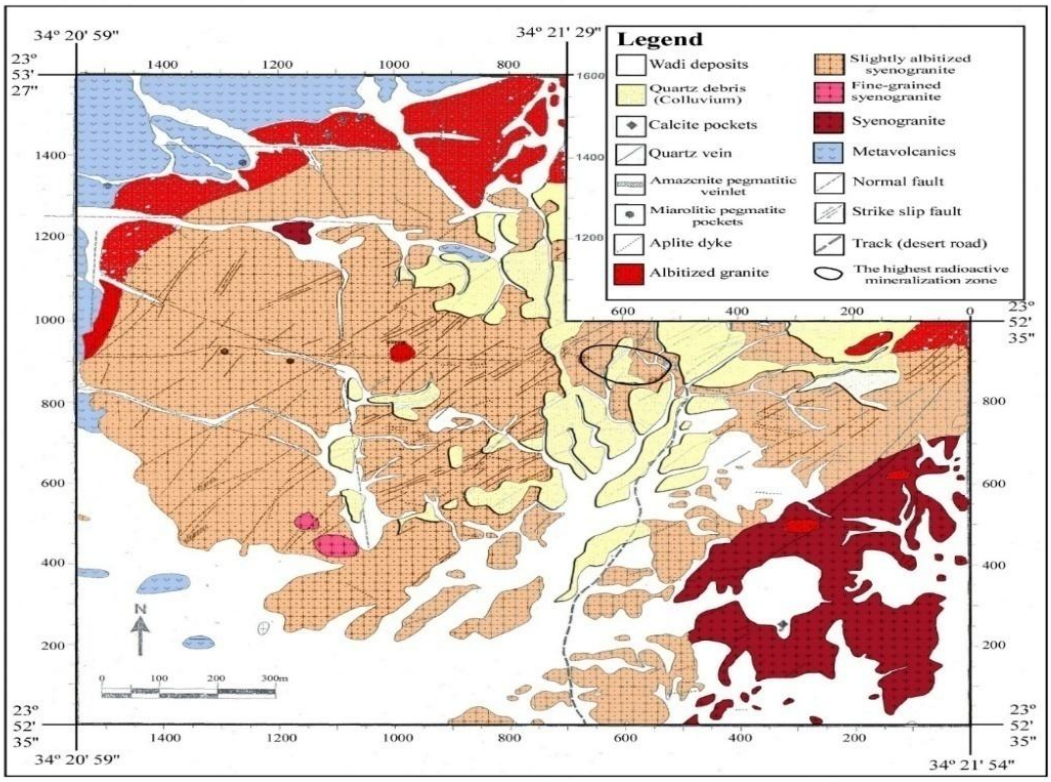

(C)

Detailed geological map of the hydrothermally altered northern part of G.El Nekeiba area, (The in set rectangle of Fig.1B), Southeastern Desert, Egypt (after Abdala et al., 2010).

Radioactivity:

The average contents of uanium (eU) for the studied altered granites are greater than the previously values recognized by Darnley (1982), Assaf et al. (1997) and El Mezayen et al. (2017) as 4 and 18 ppm, respectively. So, these altered rocks are considered as uraniferous ones (Table 1). It is worthy to be mentioned that these studied rocks belong to high thorium-high uranium granites, reflecting the effect of hydrothermal solution rich in radioelements. Normally, thorium is three times as abundant as uranium in rocks (Rogers and Adams, 1969). When this ratio is disturbed, it indicates a depletion or enrichment of uranium. The studied altered granite samples show eTh/eU average ratios lower than 3, suggesting the addition of uranium during secondary processes affecting the rocks Table (1).

Activity concentrations of ^{238}U, ^{235}U, ^{234}U, ^{230}Th, ^{226}Ra, ^{40}K and isotopic compositions were measured in 6 altered granite samples of radioactive mineralized zone. The ^{238}U activity concentrations range between 12784 and 36503 with an average 24516 BqKg^{-1}, ^{234}U activity concentrations range between 4362 and 19853 BqKg^{-1} with average 11937 BqKg^{-1}. ^{232}Th activity concentrations vary between 12363 and 16238 BqKg^{-1} with 15153.67 BqKg^{-1} as an average. ^{40}K ranges between 1321 and 1937 BqKg^{-1} with an average 1558.5 BqKg^{-1}. ^{235}U activity concentration ranges between 593 and 1485 BqKg^{-1} with average 1101.83 BqKg^{-1}. The world concentration limits of ^{238}U, ^{232}Th and ^{40}K are equal to 35, 30 and 400 BqKg^{-1} respectively (UNSCEAR, 2000). The studied samples have higher values relative that recorded in the UNSCEAR. Measured ^{234}U/^{238}U and ^{230}Th/^{238}U ARs range from 0.34 to 0.87 and from 0.49 to 0.72, respectively. Generally, the weathered rocks deviate from secular equilibrium due to the differences in radionuclides mobility during weathering processes. This relative mobility is believed to be 234U> 238U> 230Th, and consequently the weathered rocks are estimated to have ^{234}U/^{238}U<1 and ^{230}Th/^{238}U>1 (Chabaux et al., 2003 and Dosseto et al., 2008). As in the majority of the studied altered granite samples, the removal of uranium from granitic rocks is generally characterized by 234U/238U≤1 and 230Th/234U>1 (Latham and Schwarcz, 1987), suggesting uranium migration from these granites to the surrounding rocks during later processes. This means that there is more than one stage of uranium mineralization. The first is uranium accumulation in the studied altered granites clarified from Th/U ratio, followed by later uranium leaching from altered granites to the surrounding rocks as indicated by ^{234}U/^{238}U ratio.

A significant difference of 238U/235U ratios with respect to the natural ratio (21.7) in most of the studied samples suggests that redox plays an important role in fractionation of ^{238}U and ^{235U} (Weyer et al., 2008; Montoya-Pino et al., 2010; El Aassy et al., 2017). Theoretically, 235U is preferentially retained in oxidized species such as dissolved U6+, whereas 238U is preferentially partitioned into reduced species such as uraninite (Bigeleisen, 1996; Schauble, 2007).

Table (1): radionuclide activity concentrations and their activity ratiosof highest radioactive mineralization zone in the studied granites:

Nuclide	4	5	6	4\	5\	6\
^{238}U series						
^{234}Pa	12784±31	33993±201	22765±417	16744±629	36503±938	24307±978
^{234}U	4362	11596	19853	___	___	___
^{230}Th	6241	18464	16399	___	___	___
^{226}Ra	9105	35159	19773	17645	40042	21672
^{214}Pb	10442	33544	20121	15974	36485	21930
^{214}Bi	10985	33407	20456	15762	36301	21897
^{210}Pb	5287	12372	14316	___	13112	13388
^{238}U	**12784**	**33993**	**22765**	**16744**	**36503**	**24307**
^{232}Th series						
^{228}Ac	12275±19	15254±17	15081±37	15779±65	16377±86	16411±91
^{208}Tl	12451±25	15151±15	15187±49	15550±60	16188±75	16140±115
^{232}Th	**12363**	**15202**	**15134**	**15665**	**16283**	**16275**
^{235}U	593	1452	1076	772	1485	1233
^{40}K	1321	1448	1356	1708	1641	1937
238U/235U	21.56	23.41	21.16	21.69	24.58	19.71
234U/235U	7.36	7.99	18.45	___	___	___
234U/ 238U	0.34	0.34	0.87	___	___	___
226Ra/ 238U	0.71	1.03	0.87	1.05	1.10	0.89
230Th/ 238U	0.49	0.54	0.72	___	___	___
230Th/ 234U	1.43	1.59	0.83	___	___	___
226Ra/ 230Th	1.46	1.90	1.21	___	___	___
210Pb/ 226Ra	0.58	0.35	0.72		0.33	0.62
U (ppm)	1030.97	2741.37	1835.89	1350.32	2943.79	1960.24
Th (ppm)	3060.15	3762.87	3746.04	3877.48	4030.45	4028.47
K (%)	4.22	4.63	4.33	5.46	5.24	6.19
Th/U	2.97	1.37	2.04	2.87	1.37	2.06

Mineralogical investigations

The mineralogical investigation of the studied alteredgranites is of great importance, where the distribution of chemical elements and the fractionation of some isovalents within the shear zone are mainly controlled by newly formed mineral phases. The most recorded accessory minerals include; zircon, uranothorite, kasolite, fergusonite, ferrocolumbite, galena, fluorite and gold.

Zircon ($ZrSiO_4$)

Zircon occurs as bipyramidal and/or short and long euhedral prismatic crystals, possessing various colors (pale yellow, reddish-brown, reddish-orange and colourless Fig. (1). The most common habit is the bipyramidal form with various pyramidal faces and outgrowths. The euhedral shape of the zircon suggests its magmatic origin. Some grains of the studied zircon usually show in most cases secondary growths, multiple growth and fused aggregations Fig. (2). Several zircon crystals were subjected to semiquantitative analyses using environmental scanning electron microscope (ESEM) and the EDAX analyses confirms the chemical composition of zircon. The major elements in zircon include Zr (66.94 %), Si (23.6%), Fe (1.77 %), Ca (1.43%) and Hf (3.17%). Darkening in colour of zircon may be attributed to the radiation damage resulting from their contents of Th and U in zircon crystals.

Zircon-uranothorite association

The ESEM data reflects the chemical composition of zircon and its uranothorite inclusions Fig. (2). EDAX analysis showed that, zircon is isostructural with thorite and large part of thorium is incorporated in the zircon structure as reported by Rankama and Sahama (1955) which indicates the presence of intermediate solid solution between zircon and uranothorite with different levels of substitution. The EDAX analysis indicate that uranothorite is Fe-rich and consists essentially of ThO_2, ZrO_2, CaO, Y_2O_3 and SiO_2.

Uranothorite [(Th, U) SiO_4]

The studied uranothorite generally occurs as an hedral opaque mineral grains varying in colour from dark brown to black and exhibiting submetallic to greasy luster Fig. (3). Some of them give yellowish tarnish on the surface of the grains.

From the ESEM analyses of some uranothorite mineral grains, it is indicated that they are composed mainly of ThO_2 and SiO_2 with appreciable amounts of UO_2 and Y_2O_3. Trace amounts of Al_2O_3, CaO and Fe_2O_3 are present Fig. (3).

Fluorite (CaF_2)

Fluorite commonly occurs in hydrothermal, pegmatitic and pneumatolitic veins, in greissens, in cavities of granites and occasionally in carbonate rocks and phosphorites. Investigations of granitic samples under binocular microscopes indicate that fluorite varies in color from colorless to green, violet and occasionally black, usually as cubes and sometimes as anhedral fine crystals, Fig. (5, b). EDAX analyses indicate the composition of fluorite Fig. (5, a).

The association of uranyl silicates and fluorite may reflect the role of fluoride complexes in the formation of uranyl silicates. U^{+4} fluoride complexes are stable below PH_4 providing a significant way of U migration in reducing groundwater (Parks and Pohl, 1988).

Hydrothermal systems generally evolves from high temperature acid reducing conditions to neutral oxidizing conditions (Eugster, 1984). Close to the surface, the oxygen fugacity (FO_2) increases and consequently, the uranous fluoride complexes such as UF_4, would convert to uranyl fluoride complexes UO_2F_3 at slightly acidic to slightly alkaline medium. At the surface, the pressure decreases and PH increase because the loss of volatiles (Romberger, 1984). At these circumstances, the uranyl fluoride complexes become unstable and decomposed in the presence of silicitic acid to form uranyl silicates and fluorite at low temperature conditions.

Galena:

Lead grey galena grains with sub-metallic lustre occur with appreciable amounts. Galena grains were investigated by SEMFig. (7, a). and it was found that SiO_2, CaO and Fe_2O_3 are the main components of the studied galena, in addition to minor contents of, SO_3.

Kasolite:

Kasolite is the only uranylsilicate with major lead (Pb (UO2) (SiO4). H2 O). It is a secondary mineral and occurs as a product of the reaction of meteoric water carrying silica with earlier formed secondary uranium minerals. Rismate (1982) notes that uranium released during the alteration of pitchblende in the oxidation zone forms several generations of secondary uranium minerals, the earlier ones being enriched in lead, e.g. Kasolite and masuyite, and the later ones is poverished in lead, e.g. Uranophane, Skloalowskite and boltwoodite. Under microscope, kasolite is characterized by its reddih orange color and occurs as euhedral crystal of prismatic form or as encrustation Fig. (7, b).

The presence of kasolite was also confirmed by Environmental Scan electron microscope (ESEM).

The association of radioactive mineral kasolite with some element such Pb, Fe, Cu and U indicates its formation at intermediate temperature (mesothermal) at mesothermal environment according to (Geffory and Sarcia, 1967).

Fergusonite ($YNbO_4$)

Fergusonite occurs as sub rounded to rounded grains, with pale to dark yellow or yellowish- brown

to dark brown colour Fig. (6, a). Fergusonite is of tabular prismatic shape, as confirmed by Environmental Scanning Electron Microscope (ESEM) Fig. (6, b).

Ferrocolumbite

Minerals of the columbite–tantalite group have the general formula AB_2O_6, with the Asite occupied by Fe, Mn, and a smaller quantity of Mg, Na, and trivalent ions, and the Bsite occupied by Nb, Ta and small amounts of Ti and W. The main trends known from the literature are the isovalent substitutions Fe ↔ Mn in the Asite, and Nb ↔ Ta in the Bsite, with corresponding end members ferrocolumbite, manganocolumbite, ferrotantalite and manganotantalite (Ercit, 1994, Ercit et al. 1995).

Ferrocolumbite grains were detected in the studied samples Fig. (4). The grains are generally black in colour and possess a brilliant metallic luster under binocular microscope. The grains are present in the form of massive rounded to subrounded and range in size from 15 to 200µm. Raslan (2005, 2011) identified ferrocolumbite grains in the mineralized Abu Rushied gneiss and revealed that the grains are usually characterized by the presence of surface cavities rich in iron. Several columbite crystals have been subjected to semiquantitative analyses and the obtained SEM data show that both Nb and Fe are the essential components together with minor amount of Ta, Th, U, Na, K and Mg.

G**old**

Native gold was detected microscopically in the mineralized samples. Gold shows its distinct metallic lustre and characterized by its malleable elongate wire-like shaped form. They have high reflectivity Fig. (8).

In order to have an accurate estimation of gold concentration, the samples were subjected to fire assay measurements. This method is accurate and convenient because the result is based on the actual amount of gold in the sample on basis of metal extraction on the laboratory scale. The obtained data of fire assay Table (8) show that gold content is recorded at (1 g/t) in sample.

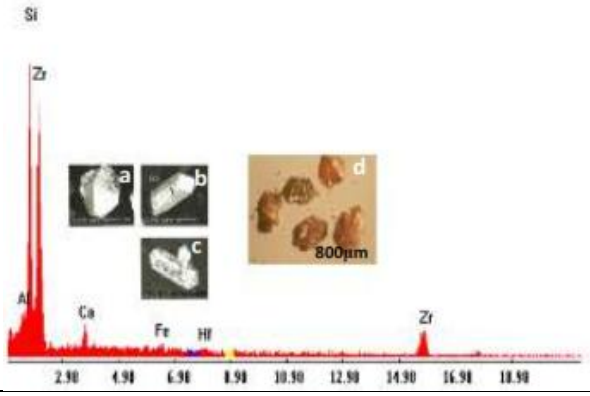

Fig. (1): BSE image and EDX spectra showing: (a) short bi-pyramid Zr, (b) long Zr, (c) outgrowth Zr and (d) showing zircon under bi-nuclear microscope.

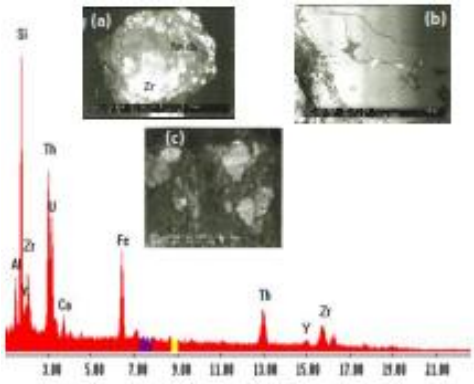

Fig (2): BSE image and EDX spectra showing:
(a) feldspar bearing Zircon and fluorite
(b) Biotite bearing Zr
(c) radioelements-bearing Zr (Uranothorite)

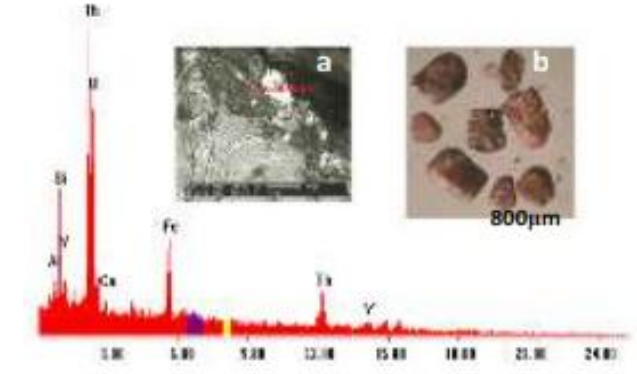

Fig. (3): a-BSE image and EDX spectra showing: Uranothorite. b- Uranothorite under bi-nuclear microscope.

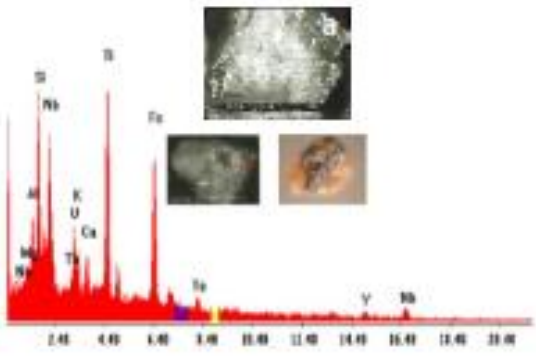

Fig. (4): a-Columbite in Mica. b- BSE image and EDX spectra showing: Ferricolumbite in feldspar. c- Ferricolumbite under bi-nuclear microscope.

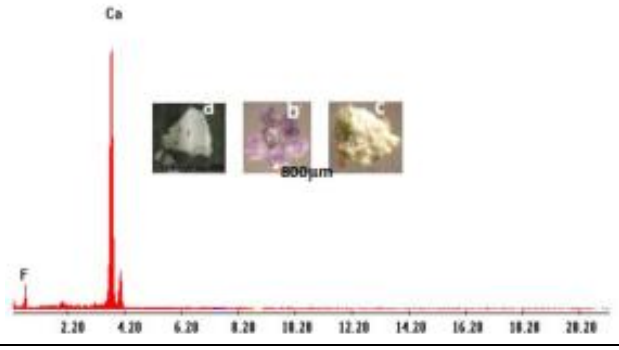

Fig (5): a- BSE image and EDX spectra showing: Fluorite (F) in feldspar (Feld). b, c- Fluorite under bi-nuclear microscope.

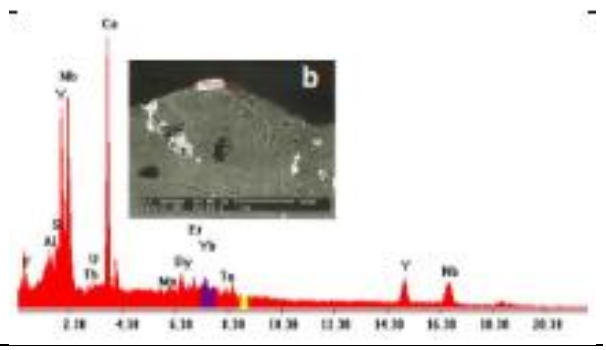

Fig (6): a-fergusonite in feldspar.
b-BSE image and EDX spectra showing fergusonite in fluorite.

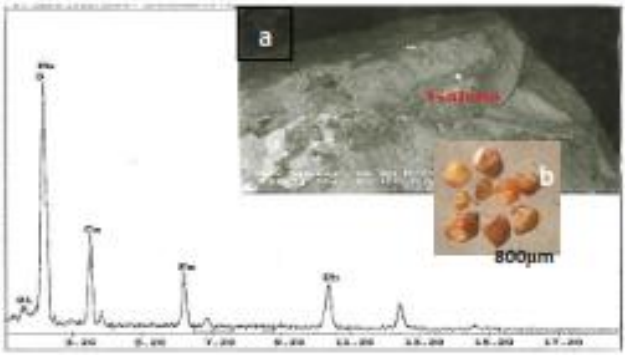

Fig. (7): BSE image and EDX spectra showing:
(a) Galena in feldspar.
(b) Kasolite under bi-nuclear microscope.

Fig. (8): Gold under bi-nuclear microscope.

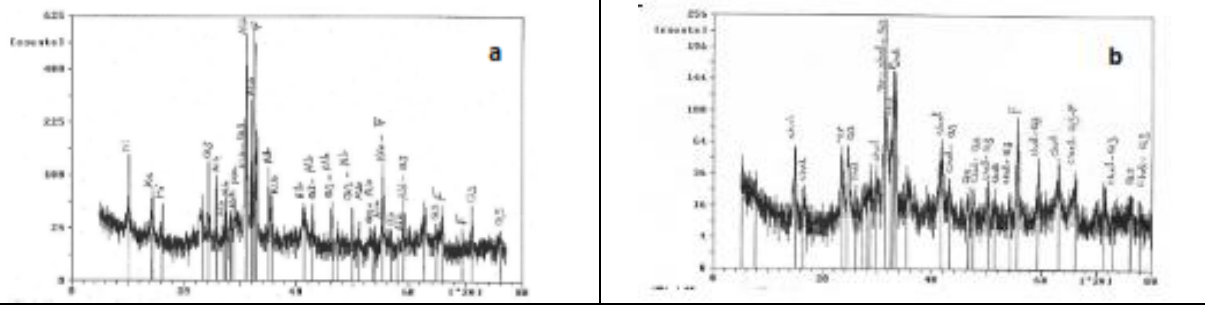

Fig (9): X-ray diffraction diagrams showing the mineral composition of studied Nikeiba granites.

(a) ASTM card: Qz –Quartz 5-0.490
Alb-Albite 10-393
F- Flourite 21-159

(b) ASTM card: Zr- Zircon 83-1374
F-Flourite 21-159
Chal-Chalcophilte 7-174

A) Major, trace elements signature:

The different types of hydrothermal alterations can be obtained by using the normative Qz-Ab-Or of Stemprok (1979) and Na_2O-K_2O variation diagram (Cuney et al., 1987). Creasy (1959) classified the hydrothermally altered rocks as argillic facies (characterized by any member of the kaolinite group) and K-silicate facies (characterized by muscovite-biotite and K-feldspar). The argillic facies was further classified by Meyer and Hemley (1967) as advanced argillic (kaolinite and montmorillonite replacing k-feldspar) and intermediate argillic (all the feldspars are converted to dicite and kaolinite).

According to the normative Qz-Ab-Or composition, the altered granitic samples could be classified into sodic, potassic, silicic and greisen Fig.

(10). In the studied altered granites, samples having high SiO_2 content are shifted towards quartz and also show imprints of greizenization as indicated by Manning (1981).

However, other samples with high Na2O contents are characterized by Na-metasomatism (desilicified samples) are shifted towards albite which is consistent with the enrichment direction of fluorine, while during Na-metasomatism, albitization proceeds through the replacement of Na^+ for K^+ and Ca^{2+} of the pre-existing feldspars but silicification results in an increase of SiO_2 at the expense of other major oxides and accompanied with increase of some trace elements such as Zr, Ba and Rb. By using the Na_2O- K_2O variation diagram (Cuney et al., 1987) Fig. (11). It is evident that the studied altered granites samples fall in desilicification, albitization and silicification fields.

Table (2): Major and trace elements concentration of the studied altered granite.

Oxide/Sample	3//	C-2	5//	6	7	8	9//	12	A-3	B-2	H-1	H-3
SiO_2	71.2	89.5	72.3	77.8	75.5	84.5	67.7	72.7	75.8	69.7	73.8	72.3
Al_2O_3	11.3	3.6	11.7	10.4	10.4	7.5	10.9	10.2	9.7	13.6	11.04	11.6
Fe_2O_3	2.8	0.58	3.6	2.7	2.2	1.3	2.6	4.1	1.9	3.1	4.2	2.8
MnO	0.13	0.02	0.08	0.035	0.11	0.065	0.07	0.06	0.03	0.085	0.12	0.1
Ti_2O	0.42	0.53	0.23	0.25	0.4	0.33	0.43	0.35	0.52	0.35	0.42	0.37
CaO	2.8	0.79	1.4	0.59	0.84	0.56	2.13	0.59	0.56	1.5	1.7	1.3
MgO	2.5	1.4	0.85	0.58	0.92	1.4	3.7	1.3	1.7	0.85	1	2.1
Na_2O	5.2	0.79	4.9	4.8	5.6	1.9	5.3	5.5	5.8	6.02	4.7	4.8
K_2O	0.43	1.5	2.7	2.11	3.2	2.3	2.4	2.7	1.5	2.5	2.3	3.4
P_2O_5	0.001	0.002	0.001	0.001	0.002	0.003	0.001	0.002	0.002	0.003	0.001	0.002
LOI	1.8	0.7	1.2	0.7	0.5	1.04	2.9	0.9	0.67	0.84	0.5	1.14
Total	98.53	99.32	98.88	99.94	99.61	100.8	98.13	98.36	98.13	98.5	99.72	99.9
Co	119	0.27	1.7	0.9	1.3	1.48	1.5	1.31	0.83	0.91	0.99	0.9
Cr	1.75	96.3	1.88	4.6	6.72	5.08	0.81	60.6	5.5	0.61	4.02	1.2
V	3.9	4	5.01	3.3	4.63	3.01	4.96	3.99	3.74	3.46	2	3.8
Cu	47.5	59	338	89.1	62.7	39.2	118	72	122	236	55.6	250
Ni	UDL	UDL	UDL	UDL	UDL	UDL	UDL	UDL	UDL	UDL	UDL	UDL
Pb	44	38.8	56.3	42.2	46.9	43.6	55.9	54.5	47.1	35.53	36.6	34
Sr	36.7	23.8	20	18.85	18.81	49.5	31.9	21.4	18.2	27.9	33.7	29.2
Zn	121	40.8	154	38.8	184.2	92.44	95.3	74.7	39.5	124.3	113	78.3
Zr	6798	1165	1981	1334	2921	8306	2407	2231	1310	739	533	590
Au	1.00											

*Au = 1.00 ppm

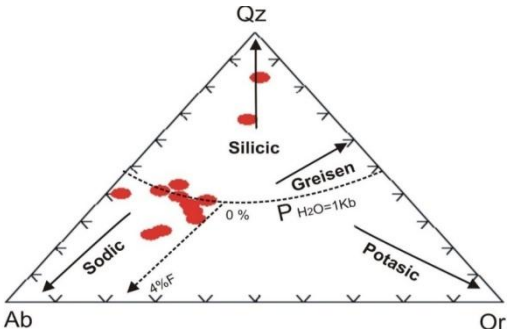

Fig. (10): Normative Qz-Ab-Or ternary diagram. The ternary minimum for 1 kb H2O pressure from Tuttle and Bowen (1958) and the stars represent the ternary minima for a granite system with 0% and 4% F (Manning, 1981). Vector A shows the migration of ternary minima as F content increases in the melt. The trends of granitic alteration types are from Stempork (1979).

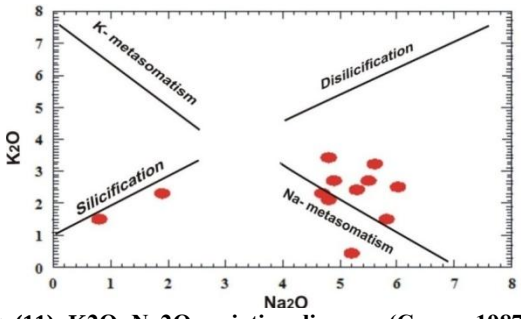

Fig. (11): K2O−Na2O variation diagram (Cuney, 1987).

Meyer and Hemley (1967) classified the K-silicate facies as: (1) propylitic (containing epidote-chlorite alteration), (2) sericitic (containing plagioclases and K-feldspars, both of which were converted to sericite and (3) potassic (characterized by the alteration of plagioclase into K-feldspar or mafic minerals into muscovite) subtypes. Altered granite

samples are plotted on the diagram () of Meyer and Hemley (1967). It is evident that most samples fall in sericite facies (due to sericitization processes).

On the (Na2O+CaO)−Al2O3−K2O ternary diagram of (Nasbitt and Young, 1989) shows that all altered granites samples plot parallel advanced weathering trend, which its initial trend parallel to the K2O−Al2O3 side-line of the diagram Fig (12).

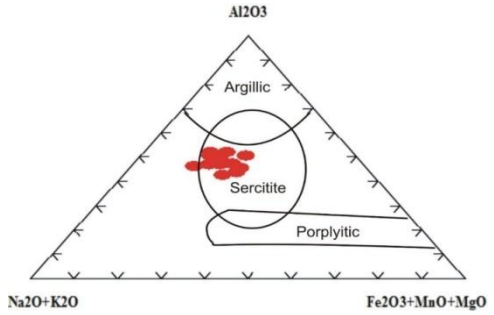

Fig (12): Al2O3− (Na2O+K2O)− (FeOT+MnO+MgO) ternary diagram (Meyer and Hemly, 1967).

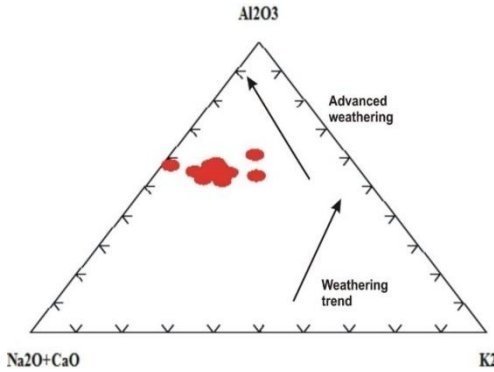

Fig (13): Al2O3− (Na2O+CaO) −K2O ternary diagram (Nasbitt and Young, 1989) for altered granitic rocks.

B) REE geochemistry and tetrad effect:

Refers to the subdivision of the 15 lanthanide elements into four groups in a chondrite normalized distribution pattern: (1) La–Ce–Pr–Nd, (2) Pm–Sm–Eu– Gd, (3) Tb–Dy–Ho, and (4) Er–Tm–Yb–Lu, and each group forms a smooth convex (M-type) or concave (W-type) pattern (Masuda et al., 1987). The values of tetrad effect were calculated according to the quantification method of Irber (1999):

t1 = (Ce/Ce*× Pr/ Pr*), t3 = (Tb/Tb*×Dy/Dy*), t4 =(Tm/Tm* ×Yb/Yb*)

Degree of the tetrad effect $T_{1,3} = (t1 \times t3)^{0.5}$.

A REE pattern that does not show a tetrad effect has values of $TE_{1.3} < 1.1$. The M-shaped pattern shows TEi > 1.1 and the W-shaped TEi < 0.9.

The REE tetrad effect is most visible in late magmatic differentiates with strong hydrothermal interactions or deuteric alteration. Moreover, the tetrad effect is often accompanied by other modified geochemical behavior of many trace elements, which is termed by Bau (1996) as non-CHARAC behavior (CHARAC =Charge-and-Radius-Controlled). Such behavior occurs typically in highly evolved magmatic systems enriched in H2O, CO2 and elements such as Li, B, F and/or Cl, which suggests the increasing importance of an aqueous like fluid system during the final stages of granite crystallization (Bau, 1996; Irber, 1999).

The kinked pattern, which is the characteristic REE tetrad effect, according to Masuda et al. (1987), extraction of a coexisting fluid from a peraluminous melt would result in both of the M-shaped and W-shaped REE tetrad effect, the former of which would be shown in the residual melt phase and the latter of which shown in the fluid. However, this corresponding relationship for a magma system has not been observed in the natural environment. Recently, it has been argued that peraluminous magmatic systems represent the transition from a silicate melt to a high-temperature hydrothermal system, and thus, the geochemical behavior of the isovalent incompatible elements in highly evolved granitic rocks are controlled mainly by chemical complexation with a variety of ligands (Bau and Dulski, 1999; Bau, 1996, 1997; Dostal and Chatterjee, 2000). Therefore, the origin of the REE tetrad effect was ascribed to the interaction between fluorine bearing fluid and silicate melt phases (e.g., see Irber, 1999). Monecke et al., (2002), proposed that the tetrad effect might have formed within the magma fluid system before emplacement in the subvolcanic environment where phase separation caused a split of this system into fluid and magma subsystems, or that the tetrad effect might also be inherited from an external fluid influencing the system during or after the emplacement of the magma. Takahashi et al., (2002) recently found both W- and M-type tetrad effect in REE patterns for the water-rock systems in the Tono uranium deposit, central Japan, which is interpreted as that the preference of the groundwater for a W-type tetrad effect produces an M-type tetrad effect in the granitic rocks during weathering processes. It is important to notice that the reported cases are M- or W-type tetrad effects occurring separately in natural systems, however, the composite M- and W-type REE tetrad effect were firstly reported by Zhao et al., (2008). Thus, our study is important step in understanding the REE tetrad effect.

The kinks in the REE patterns are camouflaged by prominent convex and concave tetrads and pronounced negative to slightly positive Eu anomalies. The second tetrad is comparably difficult to recognize due to the anomalous behavior of Eu and the fact that

Pm does not occur in nature. Fig. (14) shows that samples of altered granites have strong M-type tetrad effect in the first and third tetrad and strong W-type tetrad effect in the fourth tetrad.

The index of tetrad effect intensity, TE1,3 and TE1,4, are higher than 1 in samples 4 & 5, respectively which implies that there was an interaction between melt and water-haloid-rich fluid when these granites are crystallized from magma. However, samples 4 & 6 show clear convex (M-type) T_3 with concave (W-type) T_4 Fig. (14) and Table (3).

ZHAO et al., (2008) suggest that the new MW-type of tetrad effect is likely to be caused mainly by the interaction of aqueous liquids with alkaline rocks. Mahdy and El Kammar, (2003) in Kab Amiri granite, CED, Egypt revised the convex (M-type) T_1 accompanying with concave (W-type) T_3 to the physico-chemical conditions that prevailed during the alkali-metasomatism of the Kab Amiri granitoids have always been changing and the alteration products vary from one place to another.

ZhenHua et al., (2010) and El-Mezayenet al., (2015) stated that the peculiar MW-type tetrad effect might be an indicator for Au mineralization of reworked plutons and this vision could be applied in the study area where, there is Au grains in the high mineralized zone granite Fig. (14) comparing with the fresh one.

Table (3): Rare earth elements concentration of highest radioactive mineralization zone in the studied granite.

REEs	4	5	6	REEs	4`	5`	6`
La	3651.4	549.9	6019.4	Tb	0.5	0.4	0.3
Ce	1692.4	180.1	1389.7	Dy	910.4	940.32	1226.1
Pr	13.2	2.76	7.56	Ho	0.1	0.1	0.1
Nd	2.93	0.9	465.74	Er	36	7.06	9.81
Sm	1	1	5.43	Tm	1.07	7.03	0.1
Eu	1.08	0.16	0.88	Yb	11.49	18.5	0.3
Gd	206.8	30.87	300.2	Lu	0.58	1.78	0.1
t1	2.039	1.414	0.086				
t3	5.101	12.002	3.806				
t4	0.795	3.335	0.181				
$TE_{1..3}$	3.225	4.119	0.573				
$TE_{1..4}$	1.273	2.171	0.125				

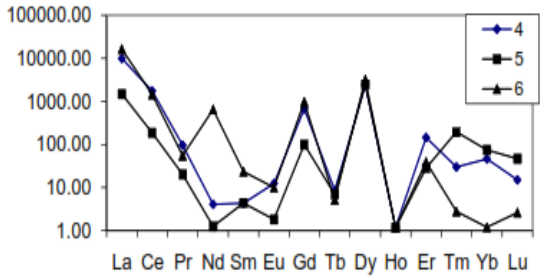

Fig. (14): Chondrite- normalized REE diagram (Boynton, 1984) for highest radioactive mineralization zone in the studiedgranite.

Mineral Chemistry

The mineral chemistry is obtained by Environmental Scan Electron Microscope (ESEM) attached with Energy Dispersive X-ray (EDX) unit using many grains of K feldspars and biotite. The analysis was carried out in scan laboratory on Nuclear Material Authority, Egypt. The chemical characteristics of mineral phases improved the understanding of mechanisms of element mobility within the crystals, atomic substitutions and chemical aspects of rock forming minerals such as, feldspar as essential minerals, biotite as mafic mineral; the columbite and zircon and secondary uranium minerals as accessory minerals.

Feldspar

Spot mineral analysis of K-Feldspar from the anomalous granite samples were carried out using the ESEM (Environmental scanning electron microscope) (Table 4), shows the chemical composition of these minerals along with their structural formula.

The property indicates the role in determining the mobility of certain radionuclides depends on either K^+ or Na^+ can be accommodated in the interlayer between the sheets of silicate and uranyl polyhedral in the structure due to the presence of property-sized coordination polyhedral for both cations (Burns, 1998). The ionic radii of Na+ (1.12 and 1.24 A^o) respectively are close to those of Ca2+ (1.06 and 1.18) so, the subistitution of Ca by Na is expected, but is controlled by charge balancing mechanisms (Sha and Chappell, 1999) Fig. (15) confirms the presence of this kind of cation substitution in the studied fields as observed in the calcification process by the hydrothermal solution where Na and K are substituted by Ca accompanying this process, some trace elements

are enriched (Nb: 31.57, Zr: 45.09 and Hf: 0.96) while the temperature increase from range 750℃ to range 1000℃ as in Fig ( ). Also, the coupled substitution of REE^{3+} or Hf and Zr with Si^{4+} to replace Ca^{2+} or Na^{+} are represented in Fig. (15).

Nelson (2013) stated that the chemical compositional variation in minerals is refered to solid solution. He postulated two main types of solid solutions; the first is omission solid solutionwhen an ion of higher charge substitutes for two lower-charged ions to maintain charge balance; occupying only one site and leaving the other site as vacant, or omitted. In this study the EDX analysis indicated enrichment of Ca^{+2} (14.14%) on the account of Na^{+1} and K^{+1}. The second type is the interstitial solid solution where some sites in the crystal structure are vacant (M-sites) and considered as voids occupied by other ions especially the trace elements such as U, Nb and Y (Table 4).

Table (4): Representative chemical composition with structure formula of Feldspars.

No*	**15**	**16**	**17**	**18**	**20**	**21**
SiO_2	65.86	57.21	65.20	19.70	65.87	43.50
TiO_2	---	---	---	---	---	---
Al_2O_3	19.13	7.02	14.6	3.94	18.76	4.23
Fe_2O_3	1.07	---	1.4	5.66	0.55	1.58
MnO	---	---	---	---	---	---
MgO	1.31	---	---	---	----	---
CaO	0.55	---	3.43	14.14	1.82	4.64
Na_2O	10.74	---	---	----	13	---
K_2O	1.35	2.32	15.73	0.69	---	---
HFO_2	---	0.49	---	---	---	0.96
ZrO_2	---	32.96	---	---	---	45.09
UO_2	---	---	---	0.70	---	---
ThO_2	---	---	---	0.57	---	---
Gd_2O_3	---	---	---	1.21	---	---
Dy_2O_3	---	---	---	2.39	---	---
Er_2O_3	---	---	---	2.38	---	---
Ta_2O_5	---	---	---	1.28	---	---
Y_2O_3	---	---	---	15.77	---	---
Nb_2O_5	---	---	---	31.57	---	---
Total	100.01	100	100.36	100	100	100
No. of cations on the basis of 8 O atoms**						
Si	2.9	2.84	3.114	0.69	2.93	3.99
AI-IV	0.99	0.42	0.823	0.16	0.98	5.32
AI-VI	---	---	---	---	---	---
Ti	---	---	---	---	---	---
Fe*	0.035	5.33	0.038	0.49	0.018	5.32
Mn	---	---	---	---	---	---
Mg	0.08	---	---	---	---	---
Ca	0.003	7.99	0.002	0.52	0.083	7.89
Na	0.9	---	---	---	0.28	---
K	0.15	0.15	0.95	0.6	---	------
HF	---	0.007	---	---	---	3.99
Zr	---	0.8	---	---	---	3.99
U	---	---	---	0.0052	---	---
Th	---	---	---	0.004	---	---
Gd	---	---	---	0.014	---	---
Dy	---	---	---	0.026	---	---
Er	---	---	---	0.026	---	---
Ta	---	---	---	0.116	---	---
Y	---	---	---	0.29	---	---
Nb	---	---	---	0.49	---	---
End-member mole %						
Or	14.2	100	99.78	53.57	---	---
Ab	85.47	---	0.21	---	77.135	---
An	0.28	---	---	46.43	22.87	100

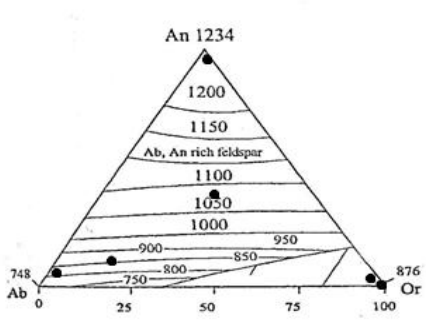

Fig (15): Plot of feldspar norms on the ternary system An-Or-Ab at 5 Kb pressure of H_2O (after dear et al., 1992).

C) Geothermometry and oxygen fugacity of biotite

Representative ESEM analyses of biotite are given in table (5), The structure formula has been calculated on basis of 22 oxygen atoms. Biotite of A-type granites are enriched in Ti, Fe and Mn and depleted in Al, Mg and K if compared with I-type granites (Abd El Rahman 1994).

Concerning the oxygen fugacity (fo2), the I type granites show the maximum oxygen fugacity with values ranging from ˜- 14 to ˜- 15, consistence with enrichment in water content, while the A-type granites were formed from reduced magma (fo2= ˜- 17), in which the temperature of crystallization biotite from the older calc-alkaline granites is higher than that of biotite from younger alkaline granites (Ivanov, 1970).

So, depending on geothermometry and oxygen fugasity, it is possible to characterize the conditions of crystallization, temperature, pressure and oxygen fugasity (fo2) of coexisting biotite in the present granites, using the Ca – $Al/_2$ – Mg diagrams of Lindsely (1983) and Nickel etal. (1985) for the analyzed data, it's clear that present granite crystalized at temperature around 800℃ of magma associated with other mafic minerals Fig. (16).

Also, the low Ti contained in biotite corresponds to low temperature of crystallization and low oxygen fugacity (Buddington and lindsley, 1946).

According, the low Ti and some samples high in Al^{VI} content in the octahedral sites of the biotite where, Al^{VI} higher in biotite formed at lower temperature due to the $Al^{VI} \rightarrow \leftarrow$ Mg and Fe^{2+} substitution, while higher temperature favour accommodation of Ti instead Al^{IV} in the biotite structure according to (Albuquerque,1973).

Suggest relatively low temperature of formation and decrease in the oxygen fugacity of the magma with decreasing temperatures of crystallization (Wones and Eugster 1965; Albuquerque,1973) then the granites were subjected to higher temperature through hydrothermal solution and mobility of minerals.

Table (5): Representative chemical composition with structure formula of Biotite:

No	11	11`	12	14	24	25
SiO_2	58.98	8.38	23.60	38	38.15	45.18
Al_2O_3	21.78	4.39	12.08	7.8	17	5.87
Fe_2O_3	6.66	21.51	---	8.9	31	12.73
CaO	1.56	1.45	3.16	1.14	---	
K_2O	1.4	---	0.78	---	11.86	5.5
Na_2O	7.01	---	5.00	---	---	---
MgO	2.62	---	6.42	---	---	---
MnO	---	6.87	---	---	---	---
TiO_2	---	1.48	17.32	---	1.21	0.85
Nb_2O_5	---	47.06	---	---	---	---
Ta_2O_5	---	8.86	---	---	---	---
UO_2	---	---	2.61	---	---	---
ThO_2	---	---	0.54	---	---	---
HfO_2	---	---	---	1.38	---	0.73
ZrO_2	---	---	---	41.45	---	29.14
No of cations **on the basis of 22 O atoms						
Si	7.41	0.43	4.55	5.87	5.56	6.64
Al^{IV}	0.59	0.27	2.7	1.42	2.44	1.006
Al^{VI}	2.43	---	---	---	0.48	---
Fe	0.63	0.82	---	1.033	3.39	1.42
Ca	0.227	0.092	0.65	0.19	---	---
K	0.227	---	0.185	---	2.21	1.3
Na	1.66	---	1.85	---	---	---
Mg	0.49	---	1.84	---	---	---
Ti	---	0.06	2.55	---	0.13	0.92
Mn	---	0.28	---	---	---	---
Ta	---	0.122	---	---	---	---
Nb	---	1.09	---	---	---	---
U	---	---	0.11	---	---	---
Th	---	---	0.023	---	---	---
Hf	---	---	---	0.06	---	0.31
Zr	---	---	---	3.11	---	2.08

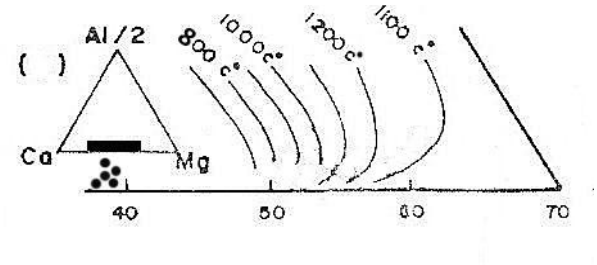

Fig (16): Ca-Al-Mg isothermal diagram of biotite after Lindsley (1983) and Nickel et al,. (1985).

4. Conclusion

G. Nikeiba is bounded by latitude (23^0 52` 35" - $23^0$ 53` 27") N and longitude (34^0 20` 59" - $34^0$ 21` 54") E covering about 400 Km^2. The rock types in Gabal Nikeiba area are dominantly metavolcanics (lithic tuffs and crystal tuffs), tonalite, granitic rocks (old granite and young granite), post granite dykes, veins and tertiary sediments. Radiometrically, the studied altered granite samples show eTh/eU average ratios lower than 3, suggesting the addition of uranium during secondary processes affecting the rocks. There is more than one stage of uranium mineralization, the first is indicted by uranium accumulation in the studied altered granites as clarified from Th/U ratio, followed by later uranium leaching as it clear uranium migration from altered granites to the surrounding rocks as indicated by $^{234}U/^{238}U$ ratio. A significant difference of 238U/235U ratios with respect to the natural ratio (21.7) in most of the studied samples suggests that redox plays an important role in fractionation of ^{238}U and ^{235}U. Theoretically,^{235}U is preferentially retained in oxidized species such as dissolved U^{6+}, where as ^{238}U is partitioned into reduced species. In the recent work 6 altered granite samples of radioactive mineralized zone, show average activity concentration of the ^{238}U (24516 $BqKg^{-1}$), ^{234}U (11937 $BqKg^{-1}$), ^{232}Th (15153.67 $BqKg^{-1}$), ^{40}K (1558.5 $BqKg^{-1}$) and ^{235}U (1101.83 $BqKg^{-1}$). The world concentration limit of ^{238}U,^{232}Th and ^{40}K are equal to 35,30 and 400$BqKg^{-1}$ respectively (UNSCEAR, 2000). The studied samples have higher values relative that recorded in the UNSCEAR., As the majoirity of the studied samples generally characterized by ^{234}U / $^{238}U \leq 1$ and ^{230}Th / $^{234}U \geq 1$, this means the first process of uranium accumulation followed by the later uranium leaching to the surrounding rocks indicated by ^{234}U / ^{238}U ratio. The geochemical characteristics studying of the altered granites show that desilicification, albitization and silicification are the main alteration features through the hydrothermal solution. chemical compositional variation in minerals is referred to two solid solution types, the first type when ion of higher charge substitutes for two lower charged ions to maintain charge balance. In this study, the EDX analysis indicate enrichment of Ca^{2+} (14.14%) on the account of Na^{+1} and K^{+1}. The second type is the interstitial solid solution, where some sites in the crystal structure are vacant (M- site) occupied by the other ions especially the trace elements such as Nb, Zr, Hf, REE and uranium, while the temperature range increase from 750^0C to 1000^0C. The studied altered granite revealed that the chondrite normalized REE patterns are different from the normal M- and W-type of tetrad effects and has complex characteristics of the two types. The first four elements (La, Ce, Pr, Nd) and the third set (Gd, Tb, Dy, Ho) exhibit a clear convex curve (M-type) while the fourth (Er, Tm, Yb, Lu) define distinct concave curves (W-type), on chondrite-normalized plots. The convex (M-type) T_1 and T_3 accompanying with concave (W-type) T_4 may be related to the physico-chemical conditions that prevailed during the alteration processes. The unusual MW-type tetrad effect could be considered as geochemical exploration method for Au mineralization of reworked plutons. Mineralogical studies indicate that the mineral association in the study area are represented by nuranothorite, thorite, kasolite, fergusonite, ferrocolumbite, zircon, gold, galena and fluorite. Depending on geothermometery and oxygen fugasity, it is possible to characterize the condition of crystallization temperature, pressure and oxygen fugasity (FO_2) of coexisting biotite in the present granite using Ca- $Al/_2$-Mg diagram of Lindsely 1983 and Nickel et.al. (1985), it is clear that the studied granite crystalized at temperature around 800^0C of magma associated with other mafic minerals.

Acknowledgments: The authors

Thanks to Dr. Prof./ Galal El Fiky, Dr. Prof./ Ehab Korny and the staff of scan electron microscope laboratory, Nuclear Materials Authority, Egypt, for their cooperation and efforts to complete and improve this manuscript.

References

1. Abdel Gawad AE (2011) Geology and radioelements potentialities of unconformable basement-sedimentary rocks at G. Nikeiba and G. Fileita Areas, South Eastern Desert, Egypt. Unpublished Ph.D. Thesis, Fac. of Sci., Minufiya Univ., Egypt. 141 p.
2. ABDEL-RAHMAN, A.M. (1994): Nature of biotites from alkaline, calc-alkaline, and peraluminous magmas. *J. Petrol.*35, 525-541.
3. Albuquerque, (1973) A.C.,1973. Geochemistry of biotites from granitic rocks, northern Portugal. Geochim. Cosmochim. Acta 37, 1779 – 1802.
4. Assaf, H. S., Mahdy, M. A., and El Afandy, A. H., 1997: Egyptian younger granites, an approach

to define parameters favoring formation of uranium deposits. 3rd Conference on Geochemistry, Alexandria Univ., pp. 409-420.
5. Bau, M. and Dulski, P. (1999): "Comparing Yttrium and Rare Earths in Hydrthermal fluid from Mid-Atlantic Ridge: Implications for Y and REE Behaviour during Near-Vent Mixing and for the Y/Ho Ratio of Proterozoic Sea Water," *Chemical Geology*, Vol. 155, No. 1-2,, pp. 77-90.
6. Bau, M., 1996. Controls on the fractionation of isovalent trace elements in magmatic and aqueous systems: evidence from Y/Ho, Zr/Hf, and lanthanide tetrad effect. Contrib. Mineral. Petrol. 123, 323–333.
7. Bau, M., 1997. The lanthanide tetrad effect in highly evolved felsic igneous rocks—a reply to the comment by Y. Pan. Contributions to Mineralogy and Petrology 128, 409–412.
8. Bigeleisen J (1996) Nuclear size and shape effects in chemical reaction. Isotope chemistry of the heavy elements. J Am Chem Soc 118:3676–3680.
9. Burns, P.C. (1998) The structure of boltwoodite and implications of solid solution toward sodium boltwoodite, The Canadian Mineralogist, 36: 1069-1075. Ivanov, 1970.
10. Chabaux F., Riotte J., Dequincey O., 2003. Uranium-series geochemistry: U-Th-Ra fractionation during weathering and river transport. Reviews in Mineralogy and geochemistry, 52, 533–576.
11. Creasy, S.C. (1959): Some phase relations in hydrothermal altered rocks of porphyry copper deposit [J.] Econ. Geol. 54, 351-373.
12. Cuney, M. and Friedrich, M. (1987) Physicochemical and crystal-chemical controls on accessory mineral paragenesis in granitoids: implications for uranium metallogenesis. *Bull. Mineral.*, 110, 235-47.
13. Darnley, A.G., 1982, "Hot granites" some general remarks. In: Maurice, Y.J. (ed.), Uranium in granites. Geol. Surv. Canada, Paper no. 81-23, pp.1-10.
14. Dosseto, A., Bourdon, B. and Turner, S.P. (2008): "Uranium-series isotopes in river materials: insights into the timescales of erosion and sediment transport," Earth and Planetary Science Letters, vol. 265, (1–2), pp. 1–17.
15. Dostal J. and Chatterjee A.K, 2000. Contrasting behavior of Nb/Ta and Zr/Hf ratios in a peraluminous granitic pluton (Nova Scotia, Canada) [J]. Chem. Geol. 163, 207–218.
16. El Shazly F. M and Krs, M 1973 Paleogeograph~ and paleomagnensm ol the Nublan Sandstone Eastern Desert of Egypt Geol Rundsch 62/l) 212—225.
17. El Aassy, Ibrahim E., El Feky, Mohamed G., El Kasaby, Mohamed. A., Ibrahim, Eman M., Salwa Sewefi, S., Attia, Reda M. (2017): Behavior of Radionuclides during Acidic Leaching Processes of Different Rock Materials, Allouga Locality, Southwestern Sinai, Egypt. International Journal of Scientific & Engineering Research, Volume 8, Issue 1, 1135-1147.
18. El Mezayen A.M, Heikal M.A, Abu Zeid I.K, El-Feky M.G, Omar S.M, Lasheen S.R (2017): Pretography, geochemistry and radioactivity of EL-Gidami granitic rocks, Central Eastern Desert, Egypt. *Al Azhar Bulletin of Science Vol. 9th., Conf., March 2017, p. 25-40.*
19. El-Mezayen, A. M, El-Feky, M. G., Omar, S. A., Ibrahim, S.A. (2015): Geochemistry and a composite M-type with W-type of REE tetrad effect in altered granites of Abu Furad area, Central Eastern Desert, Egypt. Greener Journal of Geology and Earth Sciences, Vol. 3 (2), pp. 013-029.
20. Ercit, T.S. (1994) The geochemistry and crystal chemistry of columbite group granitic pegmatites, southwest Grenville Province, Canadian Shield. Canadian Mineralogist, 32, 421-438.
21. Ercit, T.S., Wise, M.A and Cerny, P. (1995) Compositional and structural systematics of the columbite group. American Mineralogist, 80, 613-619.
22. Irber, W., 1999. The lanthanide tetrad effect and its correlation with K/Rb, Eu/Eu*, Sr/Eu, Y/Ho, and Zr/Hf of evolving peraluminous granite suites. Geochim. Cosmochim. Acta 63, 489–508.
23. Khaleal, F. M., Rashed, M. A. and Saleh, W. H. (2007): Uranium potentiality of Gabal Nikeiba Area, South Eastern Desert, Egypt. THE FIFTH INTERNATIONAL CONFERENCE ON THE GEOLOGY OF AFRICA, Vol. (1), P-P. III-41 – III-54, ASSIUT-EGYPT.
24. Latham, A.G., Schwarcz, H.P., 1987. On the possibility of determining rates of removal of uranium from crystalline igneous rocks using U-series disequilibria-1: a U-leach model, and its applicability to whole-rock data. Appl. Geochem., 2, 55–65.Montoya-Pino et al., 2010.
25. Lindsely. D.H. (1983).Pyroxene thermometry. Am. Min., 68, 477 – 493.Morimoto, N., 1988. Nomenclature of pyroxenes. Miner. Mag., V.52,pp.535 – 550.
26. Mahdy A.I. and El-Kammar A.M., 2003. Geochemical Partitioning of Isovalent and Tetrad Effect of REE Associating Episynitization of Kab Amiri Granites, Central Eastern Desert of Egypt C. pp.111–125. 5th In. Comf. of Geology of Middle East Cairo Egypt.

27. Manning, D. A. C, 1981. The effect of fluorine on liquidus phase relationship in the system Oz-Ab-Or with excess water at 1 kb. Contrib. Mineral. Petrol.76, 206–215.
28. Masuda, A., Kawakami, O., Dohomoto, Y., Takenaka, T., 1987. Lanthanide tetrad effects in nature: two mutually opposite types, W and M. Geochem. J. 21, 119–124.
29. Meyer, C. and Hemely, J.J., (1967): Wall rock alteration in geochemistry of Ore Deposits (ed. H.L. Barnes) [M]. pp.166–235. New York
30. Monecke T, Kempe U, Monecke J, Sala M, Wolf D (2002) Tetrad effect in rare earth element distribution patterns: a method of quantification with application to rock and mineral samples from granite-related rare metal deposits. Geochim Cosmochim Acta 66:1185–1196.
31. Nelson, S.A. (2013): Mineral chemistry. Tulane university. EENS2110.
32. Nickel, K.G., Brey, G.P. and Logarko, L., (1985): Orthopyroxene equilibria in the system CaO – MgO – Al_2O_3 – SiO_2 (CAMS): new experimental results and implications for two pyroxene thermometry. Contrib. Mineral. Petrol., V. 91: pp.44 – 53.
33. O' Connor, P. J., Hennessy, J., Bruch, P. M. and Williams, C. T., (1982): Abundance and distribution of uranium and thorium in the northern units of the Leinster granite, Ireland. Geol. Mag., 6: 581-592.
34. Rankama, K. and Sahama, TH. G. (1955): Geochemistry. Chicago.
35. Raslan MF and Ali MA (2011). Mineralogy and mineral chemistry of rare-metal pegmatites at Abu Rusheid granitic gneisses, South Eastern Desert, Egypt. *Geologija*, 54(2) 205–222.
36. Raslan, M.F. (2005) Mineralogy and physical upgrading of Abu Rusheid radioactive gneiss, South Eastern Desert, Egypt. The 9th International Mining, Petroleum, and Metallurgical Engineering Conference February, Faculty of Engineering- Cairo University, Min.27.
37. Rismsaite, J., 1982. The leaching of radionuclides and other ions during alteration and replacement of accessory minerals in radioactive rocks. Paper Geol. Surv. Can., 82-1B: 253.
38. Rogers, J.J.W. and Adams, J.S.S. (1969): Uranium, in Wedepohl. K.H. (ed.) Handbook of geochemistry. New York, Springer-Verlag. 4, 92 B1-92.C10.
39. Schauble EA (2007) Role of nuclear volume in driving equilibrium stable isotope fractionation of mercury, thallium, and other very heavy elements. Geochim Cosmochim Acta 71:2170–2189
40. Sha, L.K. and Chappell, B.W. (1999) Apatite chemical composition, determined by electro microprobe and laser-ablation inductively coupled plasma mass spectrometry, as a probe into granite petrogenesis, Geochimica et Cosmochimiva Acta, 63: 3861-3881.
41. Stemprok M. 1979. Mineralized granites and their origin J. Episodes. 3,20–24.
42. Takahashi, Y., Yoshida, H., Sato, N., Hama, K., Yusa, Y., Shimizu, H., 2002. W- and M type tetrad effects in REE patterns for water–rock systems in the Tono uranium deposit, Central Japan. Chem. Geol. 184, 311–335.
43. UNSCEAR, 2000a. *Sources and Effects of Ionizing Radiation. 2000 Report to the General Assembly, with scientific annexes. Volume I: Sources.* United Nations, New York.
44. Weyer S, Anbar A, Gerdes A, Gordon G, Algeo T, Boyle E (2008) Natural fractionation of 238U/235U. Geochim Cosmochim Acta 72:345–359
45. WONES, D.R. & EUGSTER, H.P. (1965): Stability of biotite: experiment, theory, and application. *Am. Mineral*. 50, 1228- 1272.
46. Zhao Z H, Bao Z W, Lee Seung-Gu (2008): A composite M- With W-type of REE tetrad effect in a north China alkaline complex. Geochim Cosmochim Acta,, 72 Supp: 11095
47. Zhao, Z.-H., Bao, Z.-W., Qiao, Y.-L., 2010. A peculiar composite M- and W-type REE tetrad effect: evidence from the Shuiquangou alkaline syenite complex, Hebei Province, China. Chin. Sci. Bull. 55, 2684–2696.

3/9/2019